Eddies in the Tropical Atlantic Ocean and their seasonal variability

H. Aguedjou, I. Dadou, A. Chaigneau, Yves Morel, G. Alory

Title : Eddies in the Tropical Atlantic Ocean and their seasonal variability

Aguedjou H. M. A.[1,3,*], Dadou I.[1,*], Chaigneau A.[1,2,3], Morel Y.[1], Alory G.[1]

[1] Laboratoire d'Études en Géophysique et Océanographie Spatiale (LEGOS), Université de Toulouse, CNES, CNRD, IRD, UPS, Toulouse, France.

[2] Institut de Recherches Halieutiques et Océanologiques du Bénin (IRHOB), Cotonou, Benin,

[3] International Chair in Mathematical Physics and Applications (ICMPA–UNESCO Chair), University of Abomey-Calavi, Cotonou, Benin.

* micael.aguedjou@legos.obs-mip.fr , isabelle.dadou@legos.obs-mip.fr

Key points:

- Detected eddies using altimetry data present amplitudes, radii and kinergy around 1-5cm, 30- 100km and 50-100cm^2.s^{-2} in the TAO.
- Seasonal cycle of eddy properties has the highest amplitude in the NBC retroflection and in the western part of NECC.
- Barotropic instabilities are the main mechanism related to eddy generation in the western part of NECC.

Abstract:

We study mesoscale eddy characteristics in the Tropical Atlantic Ocean, using 23 years of daily altimetry sea level anomalies. Eddies are mainly generated in the eastern boundary upwellings and in the Brazil current region. They have westward propagating speed reaching 20 cm s^{-1} in equatorial area, decreasing with latitudes. They present typical amplitudes of around 1-5 cm. The largest and most energetic eddies are observed in the equatorial region, in particular in the retroflection of the North Brazil Current (NBC). The seasonal cycle of the main eddy characteristics shows a marked seasonal cycle along the NBC retroflection and along the western part of the North Equatorial Countercurrent (NECC). We propose a criterion using altimetry to analyse the mechanism responsible for eddy generation. In the NECC, we argue that eddy generation is mainly due to barotropic instability of mean surface currents whereas other mechanisms must be invoked for the NBC.

Plain Language Summary

Mesoscale eddies in the ocean are numerous quasi-circular structures having typical spatial scale from 10 to 100 km. They can be formed for example by instability of the large-scale currents. Eddies play a key role in the ocean. Indeed, the kinetic energy of ocean circulation is dominated by mesoscale eddies, which play also a significant role in the transport of water masses, heat, and biogeochemical properties (e.g. nutrients) in the ocean. They have a signature in sea surface height measured by satellite altimeters. In this work, we use satellite sea level anomalies over 23 years in the Tropical Atlantic Ocean to analyze eddy properties (size, amplitude, kinetic energy, vorticity) at the basin scale and their seasonal variability. Although they are more developed in the subtropical gyres, eddies with largest radii and higher eddy kinetic energy are found in the equatorial region, with the strongest seasonal cycle in the North Brazil Current retroflection. We used a criterion based on altimetry products to study the processes involved. In the North Equatorial Countercurrent, eastern part of the North Brazil current retroflection, eddy genesis is due to barotropic instabilities whereas inside the retroflection area other processes are suspected.

1. Introduction

The development of altimetry has fostered a more advanced understanding of the ocean circulation and revealed that mesoscale eddies are a key component of ocean dynamics that contain most of the ocean kinetic energy (e.g. *Fu et al.*, 2010). Mesoscale eddies are quasi-circular oceanic structures, in rotation, with spatial scales of the order of a few tens to several hundred kilometers. Cyclonic and anticyclonic eddies (CE and AE, respectively) have lifespans from days to months and can travel several hundreds to thousands of kilometers across ocean basins (e.g. *Chelton et al.*, 2011a). Although they can form and dissipate almost everywhere in the ocean (*Fu et al.*, 2010), long-lived eddies are preferentially formed in the eastern part of the ocean basins or along energetic large-scale currents (e.g. *Chelton et al.*, 2011a). During their formation stage, mesoscale eddies trap water-mass characteristics in their core and thus play an important role in the redistribution of physical and biogeochemical properties in the global ocean. Both through horizontal and vertical mechanisms, they can also strongly impact the primary production (e.g. *Dadou et al.*, 1996; *Chelton et al.*, 2011b; *McGillicuddy et al.*, 2016; *Rousselet et al.*, 2016) and higher trophic levels (*Logerwell and Smith*, 2001; *Domokos et al.*, 2007).

The formation of vortices can be due to several processes, including barotropic and baroclinic instabilities of large-scale currents. In the tropical Atlantic Ocean, both the Canary and Benguela Eastern Boundary Upwelling Systems (EBUS) are hotspots for the generation of mesoscale eddies (e.g. *Chaigneau et al.*, 2009; *Gutknecht et al.*, 2013; *Pegliasco et al.*, 2015) through several instability mechanisms such as interaction of the large-scale circulation with islands, topographic features, coastline geometry or strong local wind shear (e.g. *Aristégui et al.*, 1994; *Chaigneau et al.*, 2009; *Djakouré et al.*, 2014). In-situ data revealed that 40-60% of the eddies formed in the eastern Atlantic EBUS are subsurface intensified with a vertical extent down to 800 m depth (*Pegliasco et al.*, 2015). Energetic eddies are also generated in the Agulhas retroflexion and propagate westward across the south Atlantic (e.g. *Penven et al.*, 2001; *Laxenaire et al.*, 2018). In the western part of the Atlantic, the generation of large isolated warm-core vortices exceeding 450km in diameter occurs in the retroflection of the North Brazil Current (NBC) propagating toward the Caribbean Sea (e.g. *Goni and Johns*, 2003; *Fratantoni and Richardson*, 2006; *Garraffo et al.*, 2003). Likewise, the equatorial Atlantic is also the site of tropical instability waves (TIW) (e.g. *Caltabiano et al.*, 2005; *Athié and Marin*, 2008) that are formed by the horizontal and vertical shears of the zonal current systems especially between the North Equatorial Counter Current (NECC) and the South Equatorial Current (SEC), and between the SEC and the Equatorial Undercurrent (EUC) (e.g. *von Schuckmann et al.*, 2008). These TIW are also associated with coherent structures called tropical instability vortices (TIV) having typical radii of ~ 300-500km and confined in the upper thermocline (*Flament et al.*, 1996; *Willett et al.*, 2006; *Dutrieux et*

al., 2008).

All of these studies focused in particular areas, especially in coastal areas (eastern and western boundary), so that the description of mesoscale eddy properties and their seasonal variability at the scale of the tropical Atlantic Ocean (TAO) is not known. The purpose of the present study is to highlight the main physical characteristics (size, lifetime, kinetic energy, amplitude, etc.) and formation mechanisms of the eddies in the TAO as well as their seasonal variability.

2. Data and methods

2.1 Altimetry data: sea level anomaly and geostrophic current

The main dataset used in this study is the Salto/Duacs gridded product of Sea Level Anomalies (SLA) and geostrophic currents distributed by the Copernicus Marine Environment Monitoring Service (CMEMS, http://marine.copernicus.eu/). The SLA product was computed relative to a 20-year (1993-2012) mean. (See for details Duacs/AVISO+, 2014; *Pujol et al.*, 2016). This product is based on Sea Surface Height (SSH) measurements from multi-mission altimeters since 1992 optimally interpolated daily onto a 0.25°×0.25° longitude/latitude grid (*Ducet et al., 2000; Le Traon et al.*, 1998). In our study, we used SLA and geostrophic currents in the Tropical Atlantic Ocean (TAO: 70°W-16°E; 30°N-30°S) for the time period extending from January 1993 to December 2015.

2.2 Eddy detection and tracking algorithm

Mesoscale eddies were identified on the daily SLA maps, using the eddy detection algorithm developed by *Chaigneau et al.*, (2008; 2009). Eddy centers correspond to local extrema in SLA (maxima for AE and minima for CE) whereas eddy edges correspond to the outermost closed SLA contour around each detected eddy center. An eddy is considered as valid if it contains at least 4 connected grid points, which approximately corresponds to a minimal radius of ~ 20 km, given the resolution of the altimetric product. For each identified eddy, several properties can be inferred such as its amplitude (A), its equivalent radius (R), or its mean eddy kinetic energy (EKE, computed from geostrophic currents). Eddy life cycles are investigated along eddy trajectories constructed using the algorithm developed by *Pegliasco et al.*, (2015). In this study, we only retained coherent and long-lived eddies having a lifetime higher than 30 days and a median amplitude and radius greater than 1 cm and 30 km, respectively.

In order to investigate the mechanisms involved in the eddy generation and their characteristics, the relative vorticity (ζ) of the large-scale flow were computed from the gradients of

the geostrophic components (u, v) in Cartesian coordinates (x, y) as in *Chaigneau et al.*, (2008) :

$$\zeta = \frac{\partial v}{\partial x} - \frac{\partial u}{\partial y} \quad (1)$$

A barotropic instability criterion based on the gradient of the vorticity of the mean current is used. Indeed, *Rayleigh* (1880) showed that for parallel sheared currents, a necessary condition for baroropic instability is that the gradient of the vorticity field changes sign. Similar results were obtained for more complex steady currents, provided the gradient of the vorticity field is computed perpendicularly to the local current, which is the preferential direction for the growth of perturbations (*Drazin and Howard*, 1966; *Arnold*, 1965). In the present geostrophic context, the local gradient of vorticity (C) is computed as:

$$C = \nabla(f + \zeta).\vec{n} \quad (2)$$

where f is the Coriolis parameter, $\vec{n} = \overrightarrow{\nabla\psi} / \left(\left\|\overrightarrow{\nabla\psi}\right\|\right)$ is the unit vector perpendicular to geostrophic streamlines and $\psi = (-g/f).SLA$ is the streamfunction.

Barotropic instability is associated with a change in the sign of C and is thus likely to occur in regions with weak values of C.

3 Results

3.1 Mean eddy properties in the Tropical Atlantic Ocean

In the TAO, more than 32,000 vortices were detected and tracked over the study period consisting of ~52% of CE and ~48% of AE. Figure 1a shows the total number of eddy per square degree that were detected in daily SLA maps between 1993 and 2015. A higher number of eddies was observed in the eastern part of the TAO particularly in the Canary and Benguela EBUS where up to 3,000 eddies per square degree were identified as well as in the western boundary along the Brazilian Current (BC) and around 20°S and 20°N in the South and North Atlantic gyres. In contrast, a weaker number of eddies was observed in the equatorial region between 12°N and 12°S, as also noted in previous studies (e.g. *Chelton et al.*, 2011a; *Fu et al.*, 2010). There is no clear geographical preference for CE and AE in the TAO (not shown) as also observed in the global ocean (e.g. *Chelton et al.*, 2011a).

The spatial distribution of eddy properties in the TAO shows that eddies have amplitudes of 1 to 6cm (Figure 1b) and more than 40% of these long-lived eddies have an amplitude of ~2cm. The largest amplitudes are observed i) along the western boundary currents, ii) south of 25°S mainly associated with anticyclonic Aghulas rings that are formed at the Aghulas retroflection and propagate westward across the south Atlantic ocean (e.g. *Laxenaire et al.*, 2018).

Although most eddies have typical radii between 60 and 90 km (Figure 1.c), individual eddies can exhibit radii up to 150 km in the equatorial region (12°S-12°N). Poleward of ±12°, radii

decrease in agreement with the theoretical Rossby deformation radii (*Chelton et al.*,1998). However at mid-latitudes (~30°), the observed eddy radii are almost twice the 1st baroclinic Rossby radius of deformation, probably due to non-linear processes or eddy coalescence (*Chaigneau et al.*, 2009; *Fu et al.*, 2010). The largest eddies are observed in the western TAO along the northeastern Brazilian coast, due to the shedding of large eddies by the NBC retroflection (*Goni and Johns*, 2003; *Frantantoni and Richarson*, 2006; *Garraffo et al.*, 2003).

On average, eddies in the TAO are characterized by relatively weak EKE of less than 150 $cm^2.s^{-2}$ (Figure 1d). However, for the most energetic eddies, located between 2°N and 6°N especially in the western part of the basin near the NBC retroflection and along the northern Brazilian coast, EKE is up to 500 $cm^2\ s^{-2}$. In the Southern Hemisphere, energetic structures are located along the south eastern Brazilian coast from 24°S to 30°S. Another area with moderate EKE of ~200 $cm^2\ s^{-2}$ is located in the northern part of the Guinea Gulf along the Guinea current off the African coast. Note that the patch of relatively high EKE values centered at 15°W and 10°N is spurious and likely due to the interference of the altimeters with the Bijagós Archipelago and the surrounding region characterized by a shallow bathymetry (< 200 m depth).

3.2 Eddy generation, propagation and lifespan

Eddies are mainly generated in the EBUS (Figure 2a) and in the western boundary along the BC where the interaction with the topography and the Brazilian coastline is a favorable condition for eddy genesis (*Soutelino et al.*, 2011). Also, an additional area of favorable eddy genesis appears in the North Atlantic subtropical gyre between 12°N and 30°N. No counterpart exists for the South Atlantic subtropical gyre. The longest-lived eddies are those generated in the subtropical gyres, especially in the Southern Hemisphere where on eddies live 150 days (Figure 2d). Statistics show that the mean eddy lifespan in the TAO is of 100 days whereas ~40% of the eddies have a lifetime of less than 50 days. Due to the β-effect, almost all the TAO eddies propagate westward (*Cushman Roisin*, 1994). Equatorial eddies move faster than off equatorial eddies with propagation speeds of 15-30 $cm.s^{-1}$ (Figure 2d).

Based on the results seen in Figure 1a, we further divide the TAO in 3 subregions to examine the mean temporal evolution of eddy properties during their life-cycle: the northern region (12°N-30°N), the equatorial region (12°S-12°N) and the southern region (12°S-30°S). In general, mesoscale eddies show a growing phase during which their amplitudes, EKE and radii strongly increase. This growing phase occurs during the first 20% of their lifetime. Although the maximum values of the eddy characteristics are reached at half of the eddy lifespan, eddy properties show a plateau-like structure between 20% and 80% of their life-cycle where only slight changes are observed. During the last 20% of their life-cycle they exhibit a decaying phase during which their

amplitudes, EKE and radii strongly decrease. On average, eddy amplitudes change from ~0.5 cm to ~3 cm in all three regions (Figure 2b), and eddy radii from 30 km to 70 km in the northern and southern regions, and up to ~100 km within the central region (Figure 2e). EKE shows almost the same evolution with very weak maximum values lower than 100 $cm^2\ s^{-2}$ in the two off equatorial regions and ~500 $cm^2\ s^{-2}$ in the equatorial region (Figure 2.c).

During their lifespan, eddy normalized vorticity, which corresponds to the ratio of eddy relative vorticity to the local planetary vorticity *f*, is less than 1 and almost constant, in all three regions though 10 times higher in the equatorial region (Figure 2f). Very weak values of ~0.07 suggest that mesoscale eddies are in geostrophic equilibrium in the off-equatorial regions. In contrast, normalized vorticity values of 0.4-0.5 suggest that ageostrophic motions might be an important component of the eddy dynamics in the equatorial region between 12°N and 12°S.

3.3 Eddy seasonal variability

The seasonal cycles of eddy properties were computed in 2° x 2° boxes from the 23-year period of SLA data (Figure 3). The amplitude of these seasonal cycles was determined for each eddy property as the difference between the maximum and minimum of the 12 monthly averages. In general, for each eddy property, the seasonal cycle amplitude is enhanced in i) the western part of TAO, ii) along the 3-8°S latitude band, and/or iii) south of 24°S (Figure 3). However, the most striking features are the maximum amplitudes observed in the region (30°W-54°W; 2°N-10°N) delimited by red boxes in Figure 3. In this region, which embeds the NBC retroflection and the western part of the NECC, the seasonal cycle amplitude reaches 1,5 cm for eddy amplitude, 25 km for eddy radius and 200 $cm^2\ s^{-2}$ for EKE representing ~60%, ~33% and ~50% of the mean values, respectively. The NBC retroflection and the eastward flowing NECC exhibit a strong seasonal variability (*Johns et al.*, 1990; *Garraffo et al.*, 2003; *Fonseca et al.*, 2004) and are associated with regular eddy shedding (*Johns et al.*, 1990 *Goni and Johns*, 2001; *Garraffo et al.*, 2003). We thus now focus on this particular region.

Figure 3d-e show the number of AE and CE trajectories that were generated locally over the 23-year period and passing through each 1°x1° pixel. We further delimited 2 subregions : NECC box and NBC box (numbered 1 and 2 respectively on Figure 3d-e). Indeed, more than 85% of both AE and CE generated in NECC box have a northwestward propagation and do not propagate through the NBC retroflection area (Figure 3d-e). Those generated within the NBC box propagate northwestward along the Brazilian coast as previously observed (e.g. *Goni and Johns*, 2003; *Fratantoni and Richardson*, 2006). Both boxes exhibit a marked seasonal cycle for eddy properties, but their amplitude and phase strongly differ from one to the other. In the NECC box, AE and CE show similar seasonal variations, with maximum values in winter (December-February) and

minimum values in late spring/early summer except for radii whose minimum values are observed in August-September (Figure 4 a,b and d). Normalized eddy relative vorticity shows minimum values during spring (April-May) and maximum values in early fall (September-October) in the NECC box (Figure 4c). In the NBC box, CE do not show a significant variability in amplitude, radius, EKE and vorticity, while minimum values for AE are reached in early spring. The relatively high values of normalized vorticity in that box suggest that eddies are much more ageostrophic within the NBC retroflection.

The number of new eddies generated over the study period exhibits a strong seasonal cycle with a minimum of 1 eddy per year generated during spring (April-May) and a maximum of 3 during late summer (August- September) within the NECC box. In contrast, in the NBC box, the seasonal cycle of eddy generation is less clear, except for CE which tend to be preferentially formed in late spring and early summer (Figure 4e-f).

Figure 4e-f also display the monthly variations of large-scale relative vorticity, computed from the geostrophic currents climatology. It shows in both boxes a clear annual cycle and a weak semi-annual variability with two minima during spring and fall and two maxima in early winter and early summer. This variation is associated with variations of zonal equatorial currents especially the NECC, the northern branch of the SEC (nSEC) and with the variation of the NBC retroflection (e.g. *Garraffo et al.*, 2003; *Fonseca et al.*, 2004). Similar seasonal variability was obtained for current shear and strain using both geostrophic and total surface current climatology from drifters data (not shown).

To further investigate the mechanism that drives eddy generation, we computed the vorticity gradient of the mean climatological currents using equation (2). The eddy generation positions were superimposed on maps of this quantity for every month. Figure 5a shows the result for January. In the NECC box, it is striking that most eddies are generated in regions were vorticity gradient changes sign and is therefore close to 0. This is further underlined in Figure 5b, which shows that most of eddies form in regions of weak vorticity gradient (~55% between +/-0.2 10^{-10} $m^{-1}.s^{-1}$ and 75% between +/-0.3 10^{-10} $m^{-1}.s^{-1}$ within the NECC box). This indicates that barotropic instability, associated with the horizontal shear of the surface currents, is probably the main mechanism of eddy generation along the NECC. In contrast, despite an annual variability of the current vorticity in the NBC box, eddy formation sites show no clear tendency here (Figures 5a-b show that only 25% of eddy generation occur between +/-0.2 10^{-10} $m^{-1}.s^{-1}$). Also note vorticity is negative over most of the NBC box. Thus, unlike in the NECC box, barotropic instability cannot explain eddy generation in the NBC box and other mechanisms are necessarily involved. *Johns et al.*, (1990) suggested that eddy-shedding in the retroflection is more likely related to a local instability process. According to *Silveira et al.*, (2000), the mechanism could be baroclinic

instability. Alternatively, wave reflection (*Ma* 1996; *Castelao* 2011) or processes related to the flow force of retroflecting current (*Nof and Pichevin* 1996) have been invoked for the generation of eddies in the NBC retroflection area.

4 Conclusions

We applied an automatic eddy detection and tracking algorithm on 23 years of daily altimetry SLA to characterize mesoscale eddies in the TAO (30°N- 30°S). More than 32,000 eddy trajectories were identified and vortices are mainly generated both in the eastern part of the Atlantic ocean, especially in the two EBUS (Canary and Benguela/Angola) and in the western boundary along the Brazil current. The detected eddies present typical amplitudes, radii and EKE of around 2-5 cm, 30-100 km and 50-100 $cm^2\ s^{-2}$, respectively. The most energetic eddies are observed in the equatorial region, in particular in the retroflection of the North Brazil Current. They propagate westward almost zonally during several weeks, with velocities reaching 20 $cm\ s^{-1}$ in the equatorial band, and less than 5 $cm\ s^{-1}$ at higher latitudes. On average, mesoscale eddies show i) a growing phase during the first 20% of their lifecycle during which their amplitude, radius and EKE strongly increase; ii) a mature phase between 20% and 80% of their life cycle during which they maintain their characteristics; iii) a decaying phase during the last 20% of their lifecycle during which their properties decrease and they dissipate.

The seasonal cycle of the main eddy characteristics shows marked seasonal variations in specific regions of the TAO, and in particular in the NBC retroflection and along the western part of the NECC. In these regions, the seasonal variability of the eddy amplitudes, radii and EKE account for about 60%, 35% and 50% of their mean values, respectively. The more significant result is that along the NECC, east of the NBC retroflection, mesoscale eddies are likely generated by barotropic instabilities due to horizontal shear of the large-scale currents. In contrast, in the NBC retroflection region, other processes, such as baroclinic instabilities, have to be involved in eddy generation. These processes, related to the vertical structure of the stratification and currents, can not be assessed with altimetry data alone. Future studies based on a combination of satellite measurements and in-situ data or on high-resolution modelling should be conducted to determine the physical mechanisms responsible for the eddy generation in the NBC retroflection.

Acknowledgments:

This work was supported by the Alti-ETAO project founded by the French National Center for Space Studies (CNES) through the Ocean Surface Topography Science Team (OSTST) and supported by the French National Institute of Sciences of the Universe (INSU/CNRS). This work is also a contribution to the junior team “SAFUME” associated with the French National Research

Institute for Development (IRD). M. Aguedjou was supported by a PhD fellowship from the IRD and the Cultural Cooperation and Action Service (SCAC) of the French Embassy in Benin. We thank Xavier Carton for useful discussions.

The gridded altimetry data were produced by SSALTO/DUACS and distributed by the Copernicus Marine Environment Monitoring Service (http://marine.copernicus.eu/)

References:

Aristégui, J., Sangra , P., Hernandez-Leon, S., Canton, M., Hernandez-Guerra, A., & Kerling, J. L. (1994), Island-induced eddies in the Canary islands, Deep Sea Res. Part Oceanogr. Res. Pap., 41(10), 1509–1525, doi:10.1016/09670637(94) 90058-2.

Arnold, V. I., (1965) : "On the conditions of nonlinear stability of plane steady curvilinear flows of an ideal fluid," Dokl. Akad. Nauk SSSR, 162, 975. In Russian.

Athié, G & Marin, F. (2008), Cross-equatorial structure and temporal modulation of intraseasonal variability at the surface of the tropical Atlantic Ocean, J. Geophys. Res., 113, C08020, doi :1029/2007JC004332.

Caltabiano, A. C. V., Robinson, I. S., & Pezzi, L. P. (2005), Multi-year observations of instability waves in the Tropical Atlantic Ocean Ocean Science Discussions, 2 , pp. 1-35.

Castelao, G. (2011), "The Internal Structure, Seasonality, and Generation Mechanisms of Surface North Brazil Current Rings". Open Access Dissertations. Paper 703.

Castellanos, P., Pelegrí, J. L., Campos, E. D., Rosell-Fieschi, M. & Gasser, M.(2015) Response of the surface tropical Atlantic Ocean to wind forcing, Progr.Oceanogr., 134, 271-292.

Chaigneau, A., Gizolme, A., & Grados, C. (2008), Mesoscale eddies off Peru in altimeter records: Identification algorithms and eddy spatio-temporal patterns, Prog. Oceanogr.,79(2–4), 106–119,doi:10.1016/j.pocean. 2008.10.013.

Chaigneau, A., Eldin, G. & Dewitte, B. (2009), Eddy activity in the four major upwelling systems from satellite altimetry (1992–2007), Prog. Oceanogr., 83(1–4),117–123, doi:10.1016/j. Pocean.2009.07.012

Chelton D. B., Peter, G., Michael, G. S., Jeffrey, J. E., & Roger, M. S. (2011), The Influence of Nonlinear Mesoscale Eddies on Near-Surface Oceanic Chlorophyll, Science 334 , 328

Chelton, D. B., Schlax, M. G., & Samelson, R. M. (2011), Global observations of nonlinear mesoscale eddies, Prog. Oceanogr., 91(2), 167–216, doi:10.1016/j.pocean.2011.01.002

Chelton, D. B., deSzoeke, R. A., Schlax, M. G., El Naggar, K. & Siwertz N. (1998), Geographical Variability of the First Baroclinic Rossby Radius of Deformation, J. Phys.Oceanogr., 28(3), 433–460

Cushman-Roisin, B. (1994), Introduction to Geophysical Dynamics. Prentice-Hall, Upper Saddle River, NJ. 320 pp.

da Silveira, I. C. A., Brown, W. S., & Flierl, G. R. (2000), Dynamics of the North Brazil current

retroflection region of the Western Tropical Atlantic Experiment observations. J. Geophys. Res. 105, 28,559-28,583.

Dadou I., Garçon, V. , Andersen, V. , FlierI, G. R., & Davis, C. S. (1996), Impact , of the North Equatorial Current meandering on a pelagic ecosystem: A modeling approach, Journal of Marine Research, 54, 311-342

Djakouré, S., Penven, P., Bourlès B., Veitch, J. & Koné V. (2014), Costally trapped eddies in the north of the Gulf of Guinea, J. Geophys. Res. Ocean, 119, 6805-6819, doi : 10,1002/2014JC010243 .

Domokos, R., Seki, M. P., Polovina, J. J., & Donald, R. H. (2007), Oceanographic investigation of the American Samoa albacore (Thunnus alalunga) habitat and longline fishing grounds. Fish. Oceanogr. 16 (6), 555–572.

Drazin, P. G., & Howard, L. N. (1966). Hydrodynamic Stability of Parallel Flow of Inviscid Fluid. Editor(s): G.G. Chernyi, H.L. Dryden, P. Germain, L. Howarth, W. Olszak, W. Prager, R.F. Probstein, H. Ziegler, Advances in Applied Mechanics, Elsevier, Volume 9, 1-89.

Ducet N., P.-Y Le Traon., & Reverdun, G. (2000), Global high-resolution mapping of ocean circulation from TOPEX/Poseidon and ERS-1 and -2, J. Geophys. Res. 105 (C8), 19,477-19,498.

Dutrieux, P., Menkes, C. E., Vialard, J., Flament, P. & Blanke, B. (2008). Lagrangian study of tropical instability vortices in the Atlantic. J. Phys. Oceanogr., 38, 400–417.

Flament, P., Kennan, A., Knox, R., Niiler, P. & Bernstein, R. (1996), The three dimensional structure of an upper ocean vortex in the tropical Pacific Ocean. Nature, 383, 610– 613.

Fonseca, C. A., Goni, G. J., Johns, W. E., & Campos, E. J. D. (2004), Investigation of the North Brazil Current retroflection and North Equatorial Countercurrent variability Geophys. Res. Lett., 31, p. L21304

Fratantoni, D. M., & Richardson, P. L., (2006), The evolution and demise of North Brazil Current rings. Journal of Physical Oceanography 36, 1241–1264

Fu, L. L., Chelton, D. B., Le Traon, P. Y. & Morrow, R. (2010), Eddy Dynamics From Satellite Altimetry. Oceanography, 23, 14-25.

Garraffo, Z. D., Johns, W. E., Chassignet, E. P., & Goni, G. J. (2003), North Brazil Current rings and transport of southern waters in a high resolution numerical simulation of the North Atlantic. In: Goni, G.J., Malanotte-Rizzoli, P. (Eds.), Interhemispheric Water Exchange in the Atlantic Ocean. Elsevier Oceanographic Series 68, Elsevier, Amsterdam, pp. 375–409.

Goni, G. J., & Johns , W. E. (2001), A census of North Brazil Current rings observed from TOPEX/POSEIDON altimetry: 1992 – 1998, Geophys. Res. Lett., 28, 1–4.

Goni, G. J., & Johns, W. E. (2003). Synoptic study of warm rings in the North Brazil Current retroflection using satellite altimetry, in Interhemispheric Water Exchange in the Atlantic Ocean, Elsevier Oceanogr. Ser., vol. 68, edited by G. J. Goni and P. Malanotte-Rizzoli, pp. 335– 356,

Gutknecht, E., Dadou, I., Le Vu, B., Cambon, G., Sudre, J., Garçon, V., Machu, E., Rixen, T., Kock, A., Flohr, A., Paulmier, A., & Lavik, G. (2013), Coupled physical/biogeochemical modeling including O_2 -dependent processes in the Eastern Boundary Upwelling Systems: application in the Benguela, Biogeosciences, 10, 3559–3591

Johns, W. E., Lee, T. N., Schott, F. A., Zantopp, R. & Evans, R. H. (1990), The North Brazil Current retroflection: Seasonal structure and eddy variability, J. Geophys. Res., 95, 22,103– 22,120.

Laxenaire, R., Speich, S., Blanke, B., Chaigneau, A., Pegliasco, C., & Stegner, A. (2018), Anticyclonic eddies connecting the western boundaries of Indian and Atlantic Oceans, J. Geophys. Res.-Oceans, 123, 7651–7677.

Le Traon P.-Y., Nadal, F., & Ducet, N. (1998), An Improved Mapping Method of Multisatellite Altimeter Data, J. Atmos. Oceanic Technol. 15, 522-534

Ma, H. (1996), The dynamics of North Brazil Current retroflection eddies, J. Mar. Res., 54(1), 35–53.

Logerwell, E. A., & Smith, P. E. (2001), Mesoscale eddies and survival of late stage Pacific sardine (Sardinops sagax) larvae. Fish. Oceanogr. 10 (1), 13–25.

McGillicuddy Jr., D. J. (2016). Mechanisms of physical-biological-biogeochemical interaction at the oceanic mesoscale. Annu. Rev. Mar. Sci.8, 125-159

Nof, D., & Pichevin, T. (1996). The retroflection paradox. J. Phy. Oceanography, 26, 2344-2358

Penven, P., Lutjiehams, J. R. E., Marchesiello, P., Roy, C., & Weeks, S. J. (2001), Generation of cyclonic eddies by the Agulhas current in the lee of the Agulhas Bank Geophys. Res. Lett., 27 , pp. 1055-1058.

Pegliasco, C., Chaigneau, A., & Morrow, R. (2015). Main eddy vertical structures observed in the four major Eastern boundary upwelling systems: J. Geophys. Res. Oceans, 120, 6008-6033.

Pujol, M.-I., Faugère, Y., Taburet, G., Dupuy, S., Pelloquin, C., Ablain, M., & Picot, N. (2016). DUACS DT2014: the new multi-mission altimeter data set reprocessed over 20 years, Ocean Sci., 12, 1067-1090.

Rayleigh, L., 1880. On the stability or instability of certain fluid motions. Proc. Lond. Maths. Soc., 11, 57-70

Rousselet, L., Doglioli, A., Maes, C., Blanke, B., & Petrenko, A. (2016) Impacts of meso-to submesoscale features on the ocean circulation in the Coral Sea. Ocean Sciences Meeting 2016, Feb 2016, La Nouvelle-Orléans, LA, United States. Hal-01289131

Soutelino, R. G., da Silveira, I. C. A., Gangopadhyay, A., & Miranda, J. A. (2011). Is the Brazil Current eddy-dominated to the north of 20°S, Geophys. Res. Lett., 38, L03607, doi:10.1029/2010GL046276.

von Schuckmann, K., Brandt, P., & Eden C. (2008). Generation of tropical instability waves in the

Atlantic Ocean. J. Geophs Res, VOL. 113, C08034

Willett, C., Leben, R. & Lavin, M. (2006). Eddies and tropical instability waves in the eastern tropical Pacific: A review. Prog. Oceanogr., 69, 218–238.

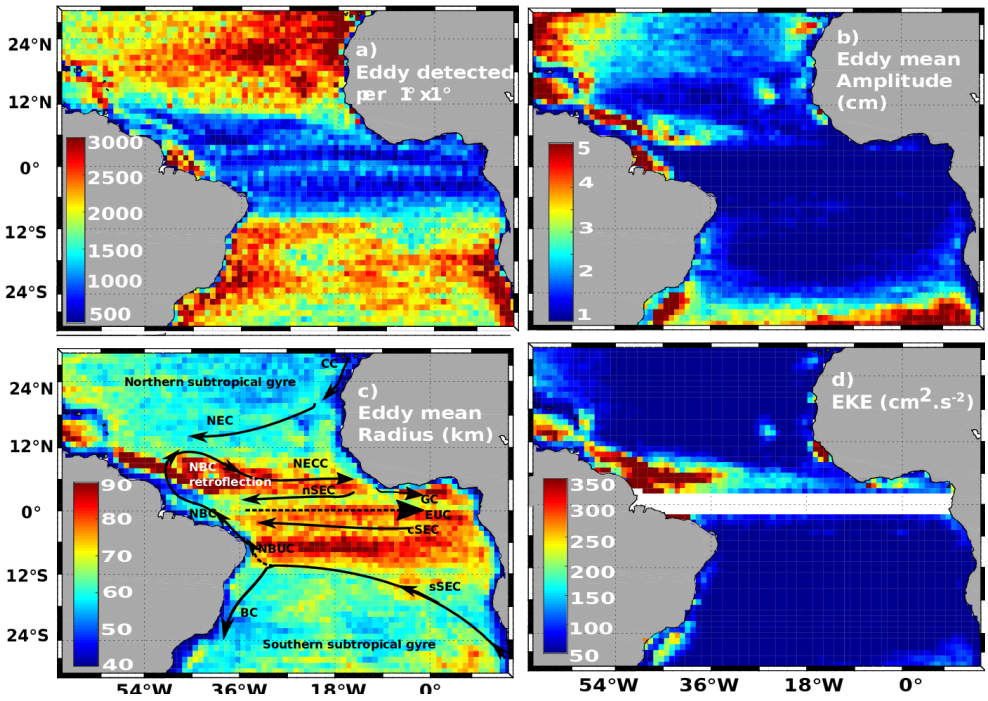

Figure 1 – Mean eddy properties over the 1993-2015 period: a) total number of detected eddies, b) eddy amplitude (cm), c) eddy radius (km) and (d) eddy kinetic energy ($cm^2\ s^{-2}$). Main currents are superimposed on figure 1c: Brazil current (BC), North Brazil Undercurrent (NBUC), North Brazil Current (NBC), Guinea Current (GC), southern, central and northern branch of South Equatorial Current (sSEC, cSEC, nSEC), North Equatorial Current (NEC), North Equatorial Countercurrent (NECC), Equatorial Undercurrent (EUC).

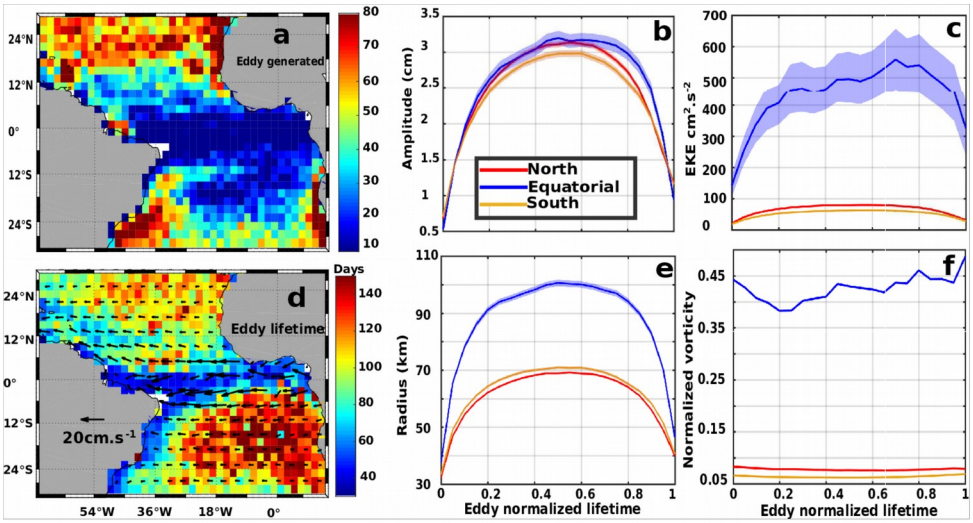

Figure 2: (a) Number of eddies generated per 2°x2° bin, and (d) eddy lifetime at birth locations (days). Arrows indicate eddy propagation speeds in cm s^{-1}. Ensemble mean (solid lines) and standard error (shading areas) of eddy (b) amplitude, (c) kinetic energy (EKE), (e) radii and (f) normalized vorticity as a function of lifetime for the long-lived eddies.

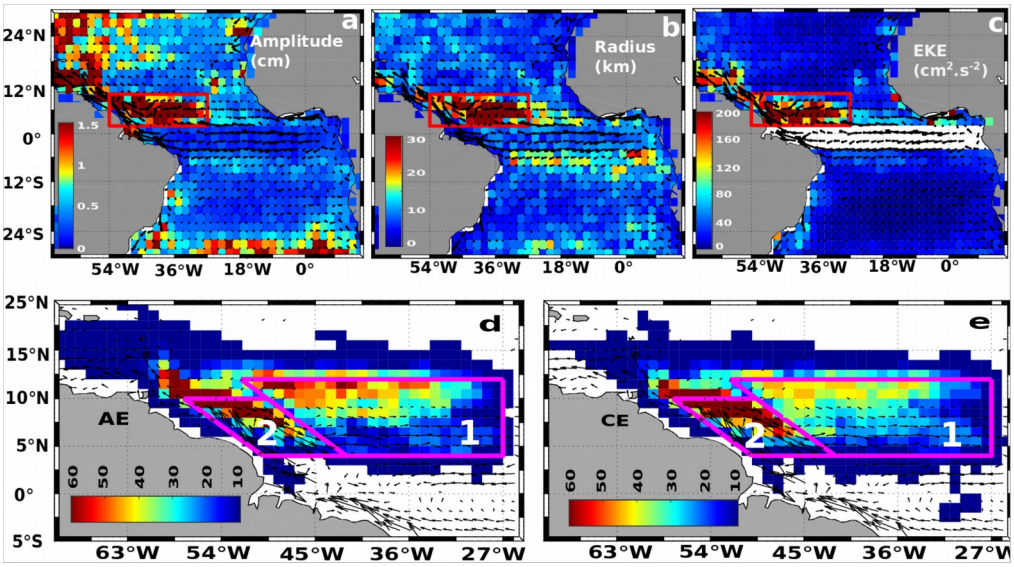

Figure 3 – Amplitude of the seasonal cycle of the a) eddy amplitudes (cm), b) eddy radii (km), c) EKE ($cm^2\ s^{-2}$). d-e) Number of AE and CE trajectories that cross each 1°x1° pixel. Black arrows represent the mean large-scale currents obtained from near-surface drifters. NECC and NBC boxes are also represented (respectively labeled 1 and 2).

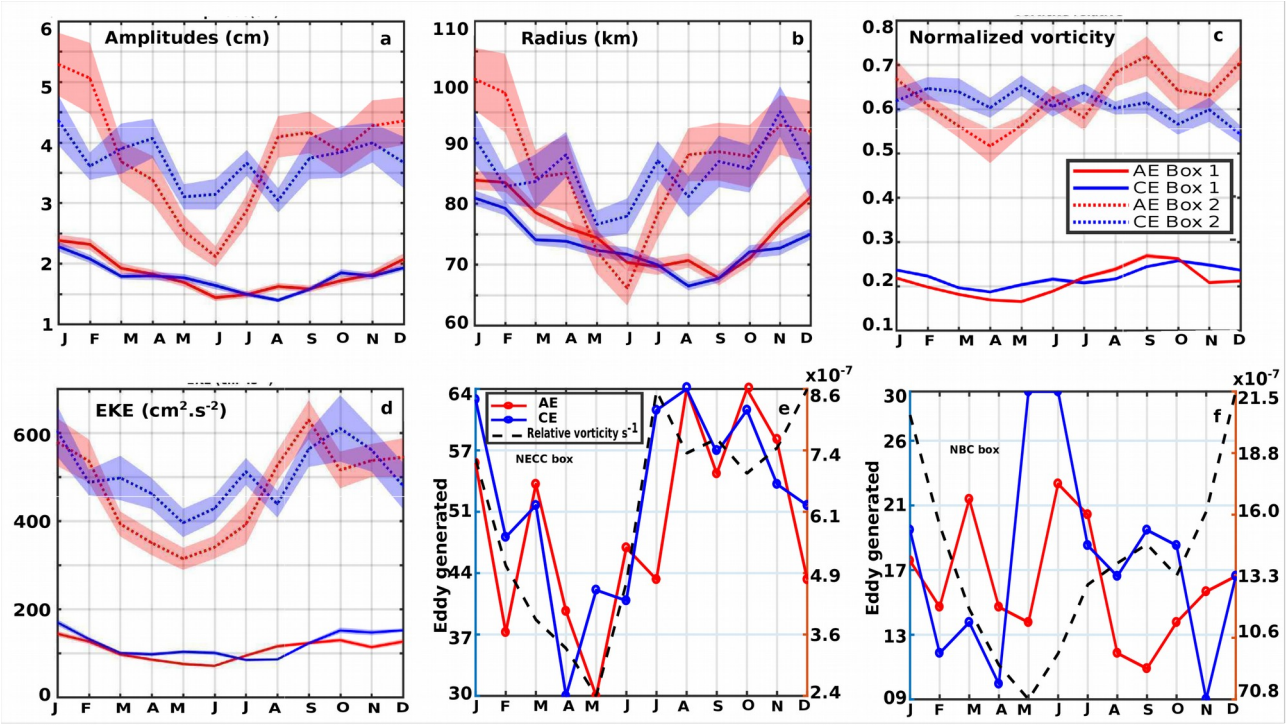

Figure 4 – Seasonal cycle of eddy properties. (a) amplitude (cm), (b) radius (km), (c) normalized vorticity, (d) EKE (cm² s^{-2}) for AE (red lines) and CE (blue lines) in NECC (solid lines- Box 1) and NBC (dotted lines- Box 2) boxes shown in Figure 3. (e, f) Monthly cumulative eddy generated and seasonal cycle of the relative vorticity of geostrophic current within NECC (Box 1) and NBC boxes (Box 2) shown in Figure 3. Shading areas are standard errors evaluated using Student's test with 95% significance level.

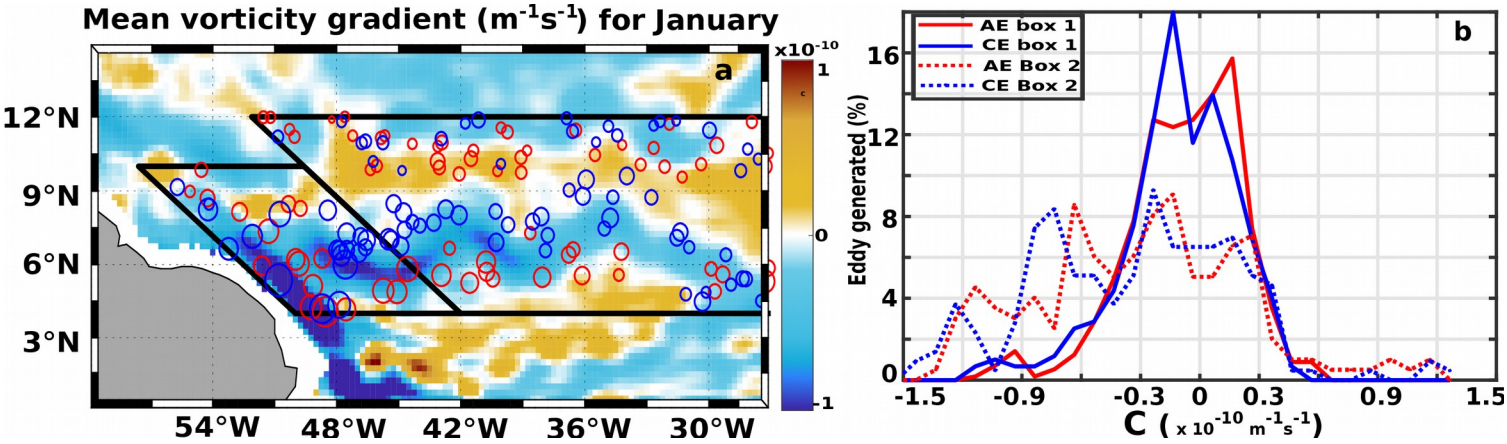

572

573 **Figure 5: (a) Mean vorticity gradient of the large-scale currents in January (color shading)**
574 **and location of the long-lived eddies generated in January between 1993 and 2015 (blue and**
575 **red circles for CE and AE, respectively). The size of circles is proportional to the mean eddy**
576 **relative vorticity. (b) Distributions of the percentage of eddies as a function of the gradient of**
577 **the large-scale relative vorticity (m^{-1} s^{-2}) at the eddy generation sites for all eddies generated**
578 **between 1993 and 2015.**

579

580